Data-driven discovery of stochastic dynamical equations of collective motion

Arshed Nabeel, Vivek Jadhav, Danny Raj M, Clément Sire, Guy Theraulaz, Ramón Escobedo, Srikanth K Iyer, Vishwesha Guttal

Data-driven discovery of stochastic dynamical equations of collective motion

Arshed Nabeel[1], Vivek Jadhav[1], Danny Raj M.[2], Clément Sire[3], Guy Theraulaz[1,4], Ramón Escobedo[4], Srikanth K. Iyer[5] and Vishwesha Guttal[1]

[1] Center for Ecological Sciences, Indian Institute of Science, Bengaluru, India.
[2] Department of Chemical Engineering, Indian Institute of Science, Bengaluru, India.
[3] Laboratoire de Physique Théorique, CNRS, Université de Toulouse – Paul Sabatier, Toulouse, France.
[4] Centre de Recherches sur la Cognition Animale, Centre de Biologie Intégrative, CNRS, Université de Toulouse – Paul Sabatier, Toulouse, France.
[5] Department of Mathematics, Indian Institute of Science, Bengaluru, India.

E-mail: arshed@iisc.ac.in, guttal@iisc.ac.in

June 2023

Abstract. Coarse-grained descriptions of collective motion of flocking systems are often derived for the macroscopic or the thermodynamic limit. However, the size of many real flocks falls within 'mesoscopic' scales (10 to 100 individuals), where stochasticity arising from the finite flock sizes is important. Previous studies on mesoscopic models have typically focused on non-spatial models. Developing mesoscopic scale equations, typically in the form of stochastic differential equations, can be challenging even for the simplest of the collective motion models that explicitly account for space. To address this gap, here, we take a novel *data-driven equation learning* approach to construct the stochastic mesoscopic descriptions of a simple, spatial, self-propelled particle (SPP) model of collective motion. In the spatial model, a focal individual can interact with k randomly chosen neighbours within an interaction radius. We consider $k = 1$ (called stochastic pairwise interactions), $k = 2$ (stochastic ternary interactions), and k equalling all available neighbours within the interaction radius (equivalent to Vicsek-like local averaging). For the stochastic pairwise interaction model, the data-driven mesoscopic equations reveal that the collective order is driven by a multiplicative noise term (hence termed, noise-induced flocking). In contrast, for higher order interactions ($k > 1$), including Vicsek-like averaging interactions, models yield collective order driven by a combination of deterministic and stochastic forces. We find that the relation between the parameters of the mesoscopic equations describing the dynamics and the population size are sensitive to the density and to the interaction radius, exhibiting deviations from mean-field theoretical expectations. We provide semi-analytic arguments potentially explaining these observed deviations. In summary, our study emphasises the importance of mesoscopic descriptions of flocking systems and demonstrates the potential of the data-driven equation discovery methods for complex systems studies.

Submitted to: *Phys. Biol.*

1. Introduction

Collective motion is a ubiquitous phenomenon in nature, observed across scales in a wide variety of systems, from microscopic organisms, insects, fish, and mammals to human crowds and even in synthetic active matter [1, 2, 3]. Collective phenomena have been a matter of investigation from the perspective of a range of disciplines beyond biology, including physics and engineering [3, 4, 5, 6, 7, 8, 9, 10]. A central question in the field of collective motion is to understand how the simple individual behavioural rules translate to the self-organised emergent dynamics of the group [1, 3, 11, 12].

To address this question, a classic and highly successful approach is that of individual-based models, where one begins with simple rules for each individual. For instance, these rules can describe how organisms align their direction of motion to that of their neighbours, and are attracted and/or repelled by them [13, 14, 15, 16, 17, 18]. Moreover, these models incorporate errors in the decision-making of organisms in the form of noise in their motion. The resulting emergent properties of the groups are then studied by computer simulations. In addition, one may analytically derive the coarse-grained description of the group properties or order parameters, such as the group polarisation, which determines the degree of directional alignment of the entire flock [19, 20, 21, 22, 23]. Unfortunately, deriving such coarse-grained models is analytically difficult except for the simplest of models [24, 25, 26]. Besides, many of the coarse-grained descriptions are accurate only when the number of individuals is very large, where the stochastic fluctuations have a negligible effect on the group dynamics.

On the other hand, many real organisms form groups that can be relatively small to medium-sized (10 to 100 individuals), an intermediate scale which we call the *mesoscopic* scale. Many experimental studies of collective motion indeed consider group sizes in this range [27, 28, 29, 30, 31, 32, 33]. At these scales, individual-level stochasticity can have observable effects at the group level, and the resulting group-level stochasticity can have unusual effects on the nature of collective motion [34, 35, 36]. This is best illustrated with a recently studied example of collective motion in karimeen fish (*Etroplus suratensis*). Here, each individual seems to copy *one* randomly chosen group member [28]. Under the assumption of such a simple behavioural rule, the analytical model predicts that the deterministic thermodynamic limit is a disordered phase, with no collective synchronised movement. However, when the coarse-grained descriptions also include the noise arising from finite size effects of the group sizes, the model predicts that collective order is possible when group sizes are smaller than a threshold group size [37]. In other words, the schooling of fish is a consequence of the noise associated with small-sized groups, and hence is termed noise-induced schooling. Similarly, other group characteristics such as mechanical properties [38, 39, 40, 41, 42] and cohesion have also been identified as a consequence of stochastic effects [43, 44]. Intrinsic noise could also be important in evolutionary dynamics that shapes collective motion of finite flocks [45, 46]. Therefore, characterising the mesoscopic description is crucial to understanding the properties of collective motion and the role of noise in finite-sized flocks [47, 37, 28].

Our current understanding of the mesoscopic descriptions of collective behaviour is

largely based on simple non-spatial models. Here, spatial correlations are absent or are neglected, and every individual of the group is equally likely to interact with every other individual of the group, an assumption equivalent to the mean-field approximation. For example, theoretical studies of mesoscopic models of collective behaviour [47, 48, 49, 37, 28, 50] ignore space (but see [51, 43]) and treat animal groups as well-mixed, i.e. any individual may interact with any other group member with equal probability. Under such assumptions, using van Kampen's system size expansion, one derives Fokker-Plank and Itô stochastic differential equations for a coarse-grained variable such as group polarisation (or degree of consensus) [52, 53]. While this mean-field approach of starting with a well-mixed, non-spatial system may be reasonable for small group sizes, as indeed confirmed by experiments on karimeen fish [28], it is unclear how it generalises to spatially explicit models of collective motion. In the spatially explicit framework, one considers individuals as self-propelled particles which interact only within a certain local radius. Furthermore, it is well known that in flocking systems there could be density fluctuations in space as well as merge and split dynamics of groups, meaning that individuals are not always uniformly spread in space [54, 1, 55, 45]. This could also mean that individuals are more likely to interact with some group members than with others depending on their position within the group. Hence, it remains unclear whether the results of mesoscopic models with non-spatial approximation apply to spatially explicit self-propelled particle models of collective motion.

In the present work, we construct a mesoscopic description of a self-propelled particle model of collective motion with spatially-explicit local interactions. Our spatial model is based on the classic Vicsek model but with two key differences: (i) the update rules are asynchronous, i.e. each individual updates its heading direction at random time points, independently from other individuals and (ii) we introduce a parameter k fixing the number of neighbours with which a focal individual interacts to align its direction of motion. This simpler version of the classic Vicsek model [15] is inspired from studies on animal collective motion, which demonstrate that many species may not be averaging over all of their local neighbours. Instead, they are likely to follow only a few of their neighbours, with various studies showing that it may be as small as one or two random (or influential) neighbours [28, 29, 30, 31, 32, 56, 57, 58, 59]. Furthermore, computational studies have demonstrated that the cognitive load to monitor the movements of a large number of neighbours is high, and they suggest that animals focus their attention on a small set of influential neighbours [60, 61, 62]. Local interaction with a few neighbours is cognitively feasible and is sufficient to maintain cohesion and order in the swarm [62, 63, 64].

At the mesoscopic regime, where one wishes to capture both deterministic and stochastic aspects of the dynamics, *stochastic differential equations (SDEs)* provide a good modelling framework to describe the group dynamics. Unfortunately, for spatial models such as ones considered in this paper, analytically deriving mesoscale SDEs starting from the individual-level interactions is a difficult endeavour. We circumvent this difficulty using a *data-driven equation learning* approach. This state-of-the-art method enables the construction of dynamical system models from the high-resolution time series of a system variable (e.g., order parameter of collective motion) [65, 66, 67]. Here, the goal is to directly discover

the governing SDEs, starting from observed (or simulated) time series, while incorporating physical constraints imposed by the symmetries of the system. The output of such an analysis is an interpretable SDE, capturing both deterministic and stochastic aspects of the dynamics, with minimum bias of the researcher modelling the data.

This paper is structured as follows. We begin with a brief review of a class of models of collective movement that ignore spatial locations of individuals in Section 2. The mesoscale SDEs for these models have been studied previously. In Section 3, we describe a generalization of these models, where interactions are localized in space, whose mesoscale descriptions are hitherto unknown. We also describe the data-driven equation discovery approach that we adopt to obtain mesoscale SDEs from these spatially explicit models. In Section 4 we discuss the results of the equation-discovery procedure—namely, mesoscopic SDEs for the spatially explicit models—highlighting similarities as well as differences from the non-spatial models. Finally, we conclude the manuscript with a brief discussion of the results and a few concluding remarks.

The main new findings of our study of the spatial models are:

- Stochastic pairwise interaction in the *local neighbourhood* can maintain high group polarisation, but only in small group sizes, via intrinsic noise-induced schooling.
- Higher order positive interactions (i.e., interacting with two or more neighbours, including Vicsek-like averaging) in the local neighbourhood can also drive schooling, but they can persist even at the macroscopic limit. This type of schooling is primarily explained via deterministic forcing terms, and is thus different from the noise-induced schooling driven by pairwise stochastic interactions.
- While the above two qualitative results are broadly consistent with the mean-field theory (MFT) based on non-spatial models, the data-derived mesoscopic equations do deviate from the MFT for the following features:
  - **A)** MFT predicts that the deterministic drift term is independent of the population size N. However, in the spatial model, the numerical coefficients of the data-derived drift function of the spatially explicit model do exhibit a dependence on N.
  - **B)** MFT predicts that the diffusion (the strength of noise) is inversely proportional to N. However, in the spatial model, this scaling relationship is sensitive to the radius of the local interaction and deviates from the MFT; especially for small to intermediate group sizes. We provide semi-analytical arguments for these observed deviations.

2. A brief review of non-spatial mesoscopic models of collective movement

We first briefly review the analytical models of mesoscopic descriptions of non-spatial flocking models, where the spatial structure is either not considered at all, or where spatial correlations between individuals are completely neglected. In such cases, mesoscale descriptions for small-sized flocks with simple interaction models may be derived analytically [37, 47]. In typical flocking models, individuals interact only with those within a certain metric or topological neighbourhood. However, in a non-spatial model, a focal

individual interacts with individuals from anywhere in the flock, irrespective of its distance from it. Hence, the spatially extended nature of the flocking system becomes irrelevant. While such non-spatial interactions may be far from reality, these models provide a good starting point for analytical derivations of mesoscale dynamics, giving us a baseline theoretical expectation to study the impact of an actual embedding space on the dynamics of the group.

We review the results of non-spatial models of flocks in a two-dimensional space from Jhawar et al [28]. In this approach, the system is fully characterized in terms of the orientation of each individual i, denoted as $\mathbf{e}_i = (\cos\theta_i, \sin\theta_i)$, where θ_i represents the heading angle of the individual. Individuals update their orientations at each time-step based on some interaction rules, as described below. For a group of N individuals, the level of *order* in the group can be characterized using a *polarisation order parameter*, defined as:

$$\mathbf{m}(t) = \frac{1}{N}\sum_{i=1}^{N} \mathbf{e}_i(t). \tag{1}$$

At mesoscopic scales—unlike in the thermodynamic limit—the inherent stochasticity in the dynamics becomes significant due to the finite number of individuals [68]. An accurate description of the system at the mesoscale should account for these stochastic effects. Therefore, we use the framework of stochastic differential equations (SDEs). Our goal is to describe the time-evolution of the order parameter $\mathbf{m}$ using a stochastic differential equation of the following form, interpreted in an Itô sense,

$$\dot{\mathbf{m}}(t) = \mathbf{f}(\mathbf{m}) + \sqrt{\mathbf{G}(\mathbf{m})} \cdot \boldsymbol{\eta}(t). \tag{2}$$

Here, $\mathbf{f}$ is a vector function called the *drift* or the force, and characterises the deterministic structure of the dynamics, e.g, the existence and stability of equilibrium points in the absence of the noise term. The function $\mathbf{G}$, called the *diffusion*, is a symmetric matrix function, and captures the stochastic fluctuations in the dynamics. The noise term $\boldsymbol{\eta}(t) \sim \mathcal{N}(0, I)$ is a Gaussian white noise vector. The square root in Eq. 2 is a *matrix square root*, i.e. $\sqrt{\mathbf{G}}$ represents the symmetric matrix $\mathbf{g}$ such that $\mathbf{g}\mathbf{g}^T = \mathbf{g}^2 = \mathbf{G}$. The functions $\mathbf{f}$ and $\mathbf{G}$ characterise the dynamics in the following way: at time t, $\dot{\mathbf{m}}(t)$ is a random vector with mean $\mathbf{f}(\mathbf{m}(t))$ and covariance matrix $\mathbf{G}(\mathbf{m}(t))$—that is, $\mathbf{f}$ characterises the mean behaviour of $\dot{\mathbf{m}}$ while $\mathbf{G}$ characterises the fluctuations. When $\mathbf{G}$ is a constant matrix with no dependence on $\mathbf{m}$, the noise is said to be *additive* or *state-independent*. When $\mathbf{G}$ depends on $\mathbf{m}$ the noise is said to be *multiplicative* or *state-dependent*.

We consider a simple class of models, where individuals can update their orientation in the following ways:

- *Spontaneous turning:* at a rate r_0, an individual may spontaneously turn and choose a random direction, i.e., the new heading angle θ_i is drawn uniformly in $[-\pi, \pi]$.
- *Stochastic pairwise interaction model ($k = 1$ interacting neighbour):* at a rate r_1, an individual may choose a random individual from the entire group, and copy its direction.
- *Stochastic ternary interaction model ($k = 2$ interacting neighbours):* at a rate r_2, in a group of 3 individuals (picked at random from the population), the most misaligned

individual takes the direction of one of the other two. This is a simplified version of alignment rules than what is seen in typical SPP models, adopted primarily to facilitate analytical coarse-graining.

Note that the orientation changes occur *asynchronously* across the individuals, at random time points determined by the corresponding rates r_0, r_1 and r_2. For the above class of models, analytical derivations of the mesoscale SDEs exist in the literature [28, 47].

For a *pairwise interaction model* with only spontaneous turns (r_0) and pairwise interactions (r_1), the mesoscale SDE takes the form [28]:

$$\dot{\mathbf{m}} = -r_0\,\mathbf{m} + \sqrt{\frac{r_0 + r_1(1-|\mathbf{m}|^2)}{N}}\, I \cdot \boldsymbol{\eta}(t). \tag{3}$$

The drift term of this equation, $-r_0\,\mathbf{m}$, is linear (like the force of a spring) and would alone lead to an exponential decay with time of $\mathbf{m}(t)$ to $\mathbf{0}$. Therefore, in the macroscopic limit $N \to \infty$, the system is in a disordered state. However, the strength of the diffusion term becomes larger for smaller N. Further, it is maximum at $\mathbf{m} = \mathbf{0}$, and decreases as $|\mathbf{m}|$ increases. Consequently, the system exhibits an order, i.e., a high polarisation with $|\mathbf{m}|$ approaching values close to 1, when the system size is less than a typical group size N_c [28, 47, 37], where $N_c \sim r_1/r_0$ and $r_0 \ll r_1$ (a regime that we will consider hereafter).

For a *ternary interaction model* with only spontaneous turns and stochastic ternary interactions (and no pairwise interactions), the mesoscale SDE has the form [37, 28]:

$$\dot{\mathbf{m}} = -r_0\mathbf{m} + r_2(1-|\mathbf{m}|^2)\mathbf{m} + \sqrt{\frac{r_0 + r_2(1-|\mathbf{m}|^2)}{N}}\, I \cdot \boldsymbol{\eta}(t). \tag{4}$$

The drift term here is cubic and has a stable manifold at $|\mathbf{m}| = \sqrt{1 - r_0/r_2}$ when $r_2 > r_0$. The diffusion term is similar to the one present in the pairwise interaction model, and is maximum at $\mathbf{m} = 0$. Here, in the macroscopic limit $N \to \infty$, the disordered state is unstable when the ternary interaction rate is higher than the spontaneous turning rate (i.e. $r_2 > r_0$). Thus, unlike the stochastic pairwise model, one can achieve the ordered state by the deterministic forces alone. We also note that the drift term here is reminiscent of the deterministic terms typically employed in the (simpler) field theories of Vicsek-class of models [1].

Finally, we note that the mean-field mesoscopic theory for the pairwise interaction and ternary interaction models predicts that the drift term is independent of the group size N, whereas the diffusion term scales inversely with N. We refer to this the scaling relationships for drift and diffusion functions.

Recall that these SDEs were derived for the nonspatial model where every individual is equally likely to interact with every other individual at all times. This assumption is strictly equivalent to the mean-field assumption, which neglects correlations between agents. In the next section, we introduce a simple spatial extension of the above interaction models, and introduce a data-driven approach to directly obtain mesoscopic SDEs from model simulations. One of our main motivations is to assess which features of the non-spatial model survive in the presence of local interactions and, possibly, strong correlations between agents.

3. Spatially explicit models and the data-driven equation discovery method

A. Local alignment models with asynchronous update rules for collective motion

We develop a simple flocking model by modifying the well known Vicsek model of collective motion [15]. In our model, each agent is characterised by its orientation, $\mathbf{e}_i = (\cos\theta_i, \sin\theta_i)$, position $\mathbf{x}_i$ and moves at a constant speed, v. Agents move within a box of length L with periodic boundary conditions, and we update the positions of agents every Δt. Recent studies have emphasised the role of the probabilistic nature of animal interactions on collective motion [69, 70, 44]. We incorporate this via asynchronous interactions among agents and choice of neighbours [70], as described below.

Analogous to the non-spatial models from the previous section, the agents in the spatial model also update their orientation by spontaneous turns, or by interacting with other individuals. The spontaneous turn event is identical to the one in the non-spatial model, where the individual spontaneously chooses a random direction, $\theta_i \leftarrow \eta$ where $\eta \sim \mathsf{Unif}[-\pi, \pi]$, with a rate r_0. In addition, an agent may also align with its neighbour(s) within an interaction radius R. We then define three models in analogy with the non-spatial models of the previous section (see also the top row panels of Fig. 1):

(i) *Local stochastic pairwise interaction model ($k = 1$ interacting neighbour):* at a rate r_1, the focal agent copies the direction of a randomly chosen neighbour from the set of neighbours that are within the interaction radius.

(ii) *Local stochastic ternary interaction model ($k = 2$ interacting neighbours):* at a rate r_2, the focal individual takes the average direction of two randomly chosen neighbours within the interaction radius.

(iii) *Local averaging model ($k =$ ALL interacting neighbours):* at a rate r_A, the focal agent takes the average direction of all neighbours within the interaction radius.

For each of the interaction models described above, the other two interactions are absent for that model. Similar to the non-spatial models, these alignment interactions happen asynchronously and stochastically, with rates r_0 (spontaneous turns), r_1 (pairwise), r_2 (ternary), and r_A (averaging). The reader might notice that the local averaging model is simply an asynchronous counterpart of the classic Vicsek model [15]. In these models, probabilistic interaction rules are implemented asynchronously across individuals, as opposed to synchronous updates at each time-step like in the Vicsek model. We choose this asynchronous variant instead of the classic Vicsek model since arguably, asynchronous updates are biologically more realistic. Furthermore, several previous studies have derived the underlying SDE for simple non-spatial pairwise and ternary stochastic models, like the ones presented in the previous section [47, 37, 48, 49]. Therefore, an asynchronous counterpart of the Vicsek model facilitates direct comparisons with the non-spatial models.

The models have the following parameters: the number of agents N, the simulation area $L \times L$, the local radius of social interaction R, the spontaneous turning rate r_0, the pairwise alignment interaction rate r_1, the ternary alignment interaction rate r_2, and the rate r_A of local-averaging among all neighbours within a radius R. We choose N in the range $5 - 80$,

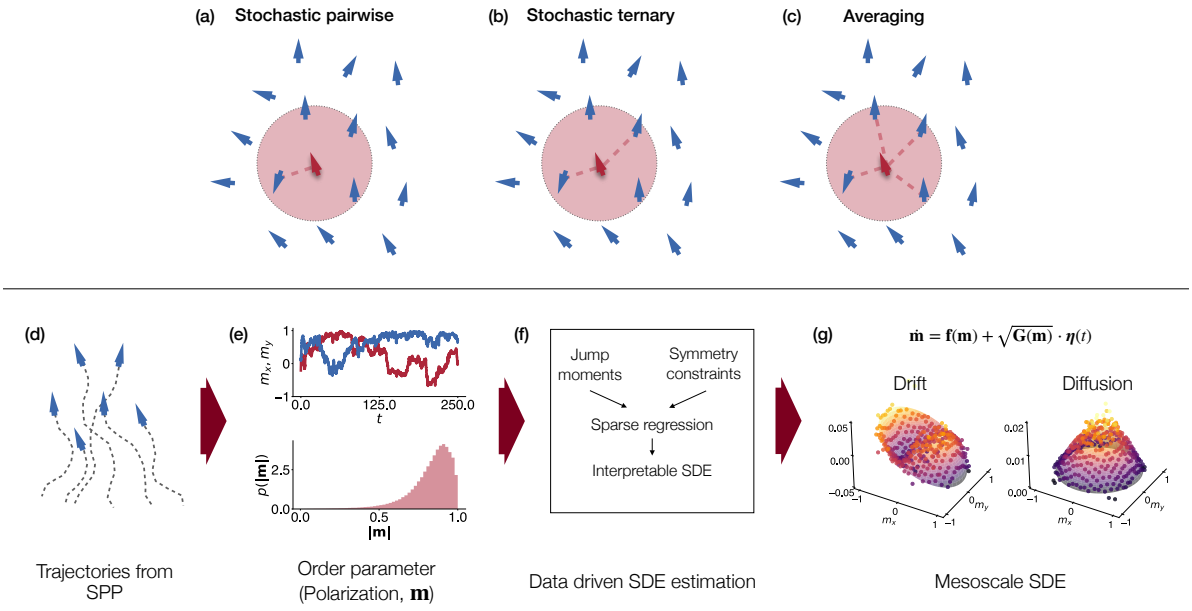

Figure 1. Schematic illustration of the simulation model (top row: a-c) and the data-driven SDE discovery procedure (bottom row: d-g). *Top Row:* Schematic of the three local-alignment interaction models of collective motion, with asynchronous update rules. Individuals interact and align their direction of motion with others present in a circle of radius of interaction R, (a) with only one randomly chosen neighbour ($k = 1$), (b) with two randomly chosen neighbours ($k = 2$) and (c) with all neighbours in the circle ($k =$ALL). *Bottom row:* (d) and (e) We simulate the model for a sufficiently long time and generate time series of the order parameter – group polarisation $\mathbf{m}$. (f) We compute jump moments and use symmetry to obtain drift and diffusion functions; we then obtain interpretable analytical functions and an SDE via sparse regression [65]. (g) A sample visualisation of SDE via drift and diffusion functions.

which covers the typical range of experimental studies. When we vary N, we consider two scenarios: a constant simulation arena size, for which we choose $L = 5$; and a constant density case, for which the density $\rho = N/L^2$ is fixed to be 1.2 particles per unit area. For most of our study, we fix $R = 1$. But to investigate the effect of R, we also study simulations with $R = 1.5$ and 2 (see *Results* section). The interaction rates were chosen so that, for $N = 30$, the average magnitude of the polarisation across the 3 models was approximately $|\mathbf{m}| \approx 0.8$. With these considerations, we choose $r_1 = 1.5$, $r_2 = 1$, and $r_A = 1.22$, and the corresponding spontaneous turning rates for the three models were $r_0 = 0.014$, 0.049, and 0.15, respectively. The movement speed v was fixed as 0.2. We reiterate that when we consider a given interaction model, the other interaction rates are zero: for example, for the ternary interaction model, the pairwise and average copying rules are absent. Each simulation begins with random orientation of individuals placed roughly at the centre of the $L \times L$ continuous two-dimensional space. The simulations continue for a duration of 10^5 time units, with asynchronous update rules [71, 72]. We assume periodic boundary conditions.

Note that the models considered here do not incorporate attraction, and hence do not explicitly enforce cohesion. This is a conscious choice, since we are interested in isolating the effect of spatial interactions on the mesoscale behaviour—introducing attraction could affect

the polarization dynamics in nontrivial ways, and is a subject for future work. Nevertheless, the specific values of parameters chosen, along with the periodic boundary conditions ensure that the group remains largely cohesive. Further, we highlight that models studied in the paper are different from other models in the literature in several important ways. First, we use asynchronous update rules which contrasts with the classic Vicsek or Couzin models where the movement updates are synchronous. Second, the SDEs studied are in the *mesoscopic* regime, where the finite number of individuals results in multiplicative noise, whose effect cannot be ignored; contrast this with hydrodynamic models of collective movement typically found in the physics literature, which are valid only in the large-N limit, where the noise is additive, or absent altogether [2, 20]. Third, as we show below, the multiplicative noise in our models is an emergent property at the group level. The randomness present at the individual level is state-independent, in contrast with other models with multiplicative noise, where even the individual-level noise is multiplicative [43].

B. Data-driven approach for deriving mesoscopic descriptions

To describe the mesoscale dynamics of the different spatial models under study, we use a *data-driven model discovery* framework. Starting from a real or simulated time series, this approach enables us to discover a governing model that describes the dynamics of the time-series. In this study, the goal is to discover stochastic differential equations that govern the polarization dynamics of the respective SPP models.

The general procedure consists of the following steps (see Fig. 1)):

- First, we generate simulated trajectories using the spatial models described above.
- Next, we quantify the dynamics of the system using an appropriate *order parameter*, which characterizes the state of the system. In our case, the order parameter of interest is the group polarisation ($\mathbf{m}(t)$, as defined in Eq 1).
- Finally, using a data-driven procedure, we find an appropriate stochastic differential equation model to describe the dynamics of the order parameter, which we describe below in more detail.

Briefly, given the polarisation time series $\mathbf{m}(t)$, sampled at some finite sampling time Δt, the first jump moment is an estimate of the drift, $\mathbf{f}$ [73]:

$$\mathbf{f}(\mathbf{m}) = \frac{1}{\Delta t}\left\langle \mathbf{m}(t+\Delta t) - \mathbf{m}(t)\right\rangle_{\mathbf{m}(t)=\mathbf{m}} \quad . \tag{5}$$

Once $\mathbf{f}$ is estimated, the diffusion can be estimated from the residuals as follows:

$$\mathbf{r}(\mathbf{m}) = \left\langle \mathbf{m}(t+\Delta t) - \mathbf{m}(t) - \mathbf{f}(\mathbf{m}(t))\cdot\Delta t\right\rangle_{\mathbf{m}(t)=\mathbf{m}} \quad , \tag{6}$$

$$\mathbf{G}(\mathbf{m}) = \frac{1}{\Delta t}\mathbf{r}(\mathbf{m})\cdot\mathbf{r}(\mathbf{m})^T. \tag{7}$$

Typically, $\mathbf{f}$ and $\mathbf{G}$ are estimated by using non-parametric methods, such as binwise averaging or kernel estimates [50, 74]. Here, to obtain interpretable representations of $\mathbf{f}$ and $\mathbf{G}$, we employ *sparse polynomial regression* to represent $\mathbf{f}$ and $\mathbf{G}$ as polynomial function [66].

Naively, one could represent $\mathbf{f}$ and $\mathbf{G}$ as component-wise as polynomial functions in m_x, m_y. However, to obtain even more parsimonious representations, one can take advantage of the inherent symmetries of $\mathbf{m}$. Specifically, since the individuals do not have a preferred direction in any of the models, $\mathbf{m}$ must exhibit rotational and mirror symmetry—the drift and diffusion functions should respect these symmetries. Therefore, the drift function can be expressed as a function of $\mathbf{m}$ and $|\mathbf{m}|$, while the diffusion function can be expressed as a function of $\mathbf{m}\mathbf{m}^T$ and $|\mathbf{m}|$. Thus, we express the discovered drift functions as a vector 'polynomial' with terms $\mathbf{m}$, $|\mathbf{m}|\mathbf{m}$, $|\mathbf{m}|^2\mathbf{m}, \ldots$, and the diffusion functions as a matrix polynomial with terms I, $|\mathbf{m}|I$, $|\mathbf{m}|^2 I, \ldots, \mathbf{m}\mathbf{m}^T, |\mathbf{m}|\mathbf{m}\mathbf{m}^T, |\mathbf{m}|^2\mathbf{m}\mathbf{m}^T, \ldots$, utilising the identity that $(\mathbf{m}\mathbf{m}^T)^{(n+1)} = |\mathbf{m}|^{2n}\mathbf{m}\mathbf{m}^T$.

The equation discovery procedure aims to represent $\mathbf{f}$ and $\mathbf{G}$ as a sparse combination of the above terms. An algorithm called STLSQ (sequentially thresholded least squares) [66] is used for sparse regression: the procedure involves iteratively fitting a regression model and eliminating terms that have fitted coefficients below a certain threshold. For more details on the regression procedure, see refs. [65, 66].

If $\mathbf{G}$ contains only $|\mathbf{m}|$-terms, $\mathbf{G}$ is a diagonal matrix and the diffusion is isotropic for all values of $\mathbf{m}$. Non-zero off-diagonal entries in $\mathbf{G}$, which in turn causes the diffusion to be anisotropic, can only appear as scalar multiples of $\mathbf{m}\mathbf{m}^T$ (see above). For the models considered here, the contribution of $\mathbf{m}\mathbf{m}^T$ terms is negligible, and can be ignored.

It is worth highlighting that the equation discovery procedure is different in spirit from simple parametric model fitting: unlike the latter case, one does not specify a model (i.e an equation) whose parameters needs to be learned—the algorithm *discovers* an appropriate model, informed by data and guided by symmetries and constrains inherent to the system.

4. Results

A. Contrast between collective motion from local stochastic pairwise interactions and higher-order interactions

In Fig. 2, we display results for three key interaction models of the spatially explicit alignment model – stochastic pairwise, stochastic ternary and Vicsek-like local averaging. We have considered a small group size of $N = 30$ to illustrate the novel features of mesoscopic dynamics. In Fig. 2, the time series of panels (a, e, i) and histogram of panels (b, f, j) of the order parameter, i.e., the group polarisation $\mathbf{m}$, show that all three models can exhibit collective motion with high directional alignment between agents. However, the underlying dynamical equations reveal interesting contrasts.

For the stochastic pairwise interaction model ($k = 1$), our data-driven discovery method yields a linear drift (Fig. 2c) and a quadratic diffusion (Fig. 2d). The corresponding mesoscopic equation for the group polarisation is

$$\dot{\mathbf{m}} = -a_1\mathbf{m} + \sqrt{a_2 - a_3|\mathbf{m}|^2}I \cdot \boldsymbol{\eta}(t), \tag{8}$$

where we interpret the SDE in the *Itô-sense*, $\eta(t)$ is a standard Gaussian white noise, and a_1, a_2, and a_3 are parameter related to the interaction rates. The values of the coefficients

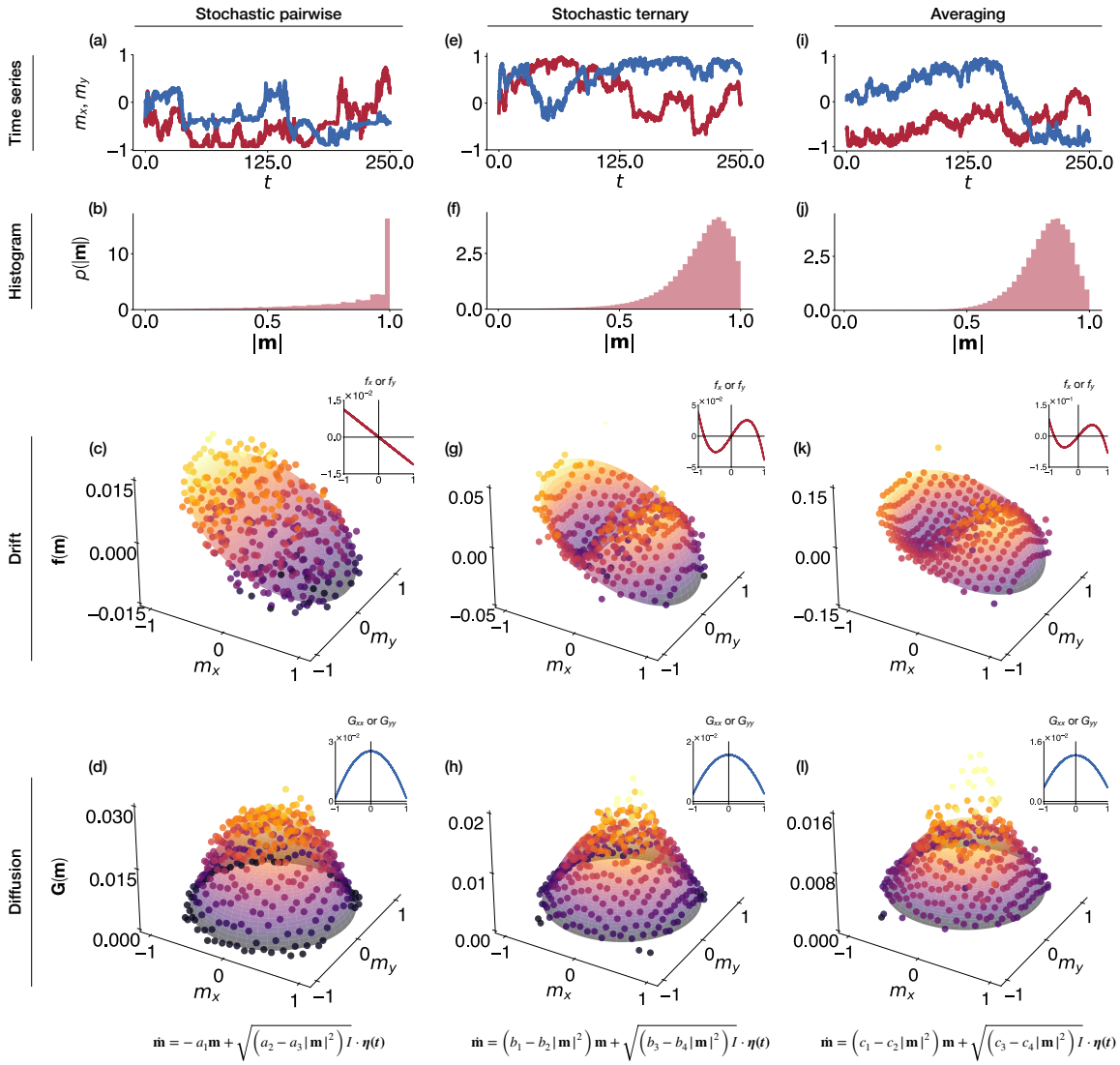

Figure 2. Estimated mesoscopic SDEs qualitatively differ between stochastic pairwise and higher-order interactions. *Top row (a, e, i)*: Sample time series of group polarisation for the three interaction models. *Second row (b, f, j)*: Histograms of the net polarisation, $|\mathbf{m}|$. We consider parameters such that all interaction models show a high degree of polarisation. *Third row (c, g, k)*: The estimated drift functions via jump moments are qualitatively different between pairwise stochastic (linear) and higher-order interactions (cubic or cubic-like with three roots). The insets show a slice along the m_x axis of the x-component f_x, i.e. $f_x(m_x, 0)$. *Fourth row (d, h, i)*: The estimated diffusion functions are all qualitatively similar. Insets show a slice along the x-axis, i.e. $G_{xx}(m_x, 0)$. The bottom row equations show the estimated mesoscopic equations as interpretable SDEs. **Parameters**: $N = 30$, $L = 5$, $R = 1$ for all three interaction models. **Estimated coefficients of SDEs**: Local stochastic pairwise: $a_1 = -0.11, a_2 = 0.023, a_3 = 0.022$. Local stochastic ternary: $b_1 = 0.081, b_2 = 0.120, b_3 = 0.016, b_4 = 0.013$. Local averaging: $c_1 = 0.171, c_2 = 0.251, c_3 = 0.012, c_4 = 0.009$.

depend on the model parameters, and the values for a typical case with $N = 30$, $R = 1$ are reported in the legend of Fig. 2. As expected, this equation has the same form as the analytically derived mean-field theoretical SDE for the non-spatial flocking model presented in [50]. This SDE suggests that, in the absence of noise, the system reaches the equilibrium $\mathbf{m} = \mathbf{0}$ and hence becomes disordered. However, the strength of the multiplicative noise is maximum when the system is in the disordered state. Furthermore, the discovered coefficients a_1, a_2, a_3 are such that the strength of the stochasticity is sufficiently high. In such cases, as reported in previous studies [47, 37, 28], the stochasticity pushes the system away from the disorder, towards the order, leading to a noise-induced high polarisation in this model. Therefore, the mesoscopic dynamics of the spatially explicit system with local pairwise interactions is qualitatively similar to the mesoscopic SDE of the corresponding non-spatial system (Eq. 3).

In contrast, we find that the mesoscopic description of the local stochastic ternary interactions ($k = 2$) is of the form:

$$\dot{\mathbf{m}} = (b_1 - b_2|\mathbf{m}|^2)\mathbf{m} + \sqrt{b_3 - b_4|\mathbf{m}|^2}I \cdot \boldsymbol{\eta}(t), \tag{9}$$

where the mathematical symbols follow the same definitions as before. The drift term is a cubic function (Fig. 2g), whereas the diffusion term is a quadratic function (Fig. 2h). Moreover, we note that $b_1 > 0$ (see caption of Fig 2 for the estimated values); thus, in the deterministic limit, the disordered equilibrium state $\mathbf{m} = \mathbf{0}$ is an unstable state whereas the ordered equilibirum corresponding to $|\mathbf{m}| = \sqrt{b_1/b_2}$ is stable. Thus, the collective motion with high polarisation is primarily driven by the drift or deterministic term. Therefore, the collective motion in ternary interaction systems can be fundamentally different from the corresponding term of the stochastic pairwise interaction system. All these observations are also true for the mesoscopic dynamics of the non-spatial ternary interactions, whose governing equation is given by Eq. 4. In other words, the mesoscopic dynamics of the spatial system with local ternary interactions are qualitatively similar to the corresponding non-spatial system. However, there are important deviations in how the diffusion term $\mathbf{G}(t)$ scales with N—a point that we explore in detail in Section 4C.

Finally, the mesoscopic description for the Vicsek-like local-averaging interaction model ($k = \text{ALL}$) has a qualitatively similar drift and diffusion as the stochastic ternary interaction system (see panels (k) and (l) in Fig. 2), with the mathematical form

$$\dot{\mathbf{m}} = (c_1 - c_2|\mathbf{m}|^2)\mathbf{m} + \sqrt{c_3 - c_4|\mathbf{m}|^2}I \cdot \boldsymbol{\eta}(t). \tag{10}$$

with $c_1 > 0$ (see the caption of Fig 2 for the estimated values); thus, like the stochastic ternary model described above, the ordered collective motion here too is driven primarily by the deterministic forces. Technically, higher order polynomials (higher than cubic) can also give a good fit for the drift function during the sparse regression. However, the higher-order terms do not change the number roots or the qualitative nature of the drift function in comparison to a cubic drift. Therefore, we constrain the fitting to cubic polynomials in our final fit, which gives the most parsimonious explanation for the qualitative shape and the stability structure of the drift function.

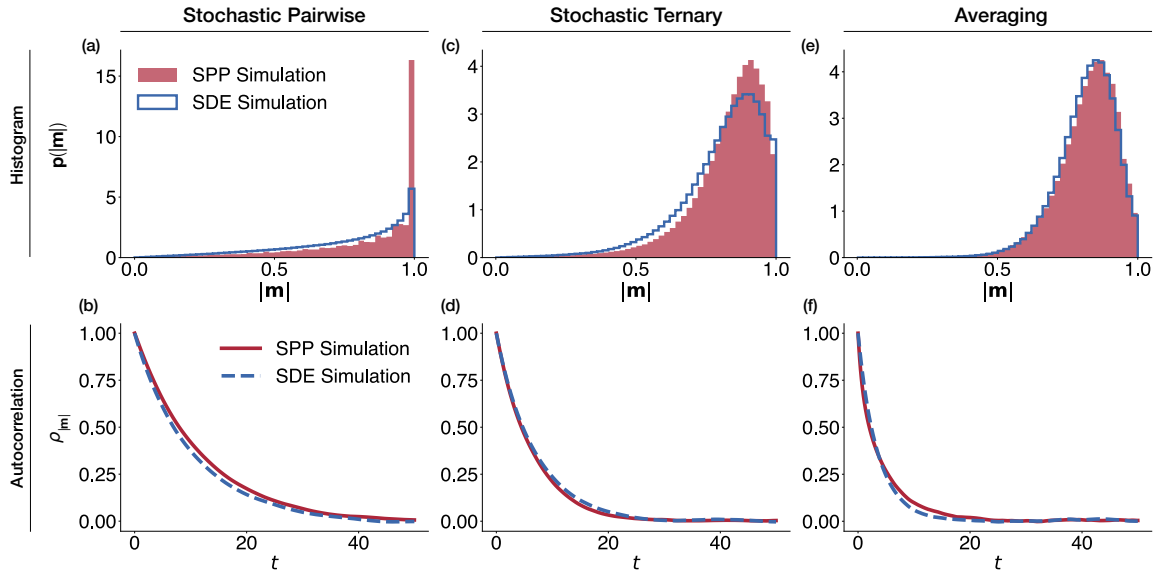

Figure 3. Consistency of the estimated SDE models. The data-driven mesoscale SDEs (Eqns 8-10) produce dynamics that closely match the actual mesoscale dynamics of the SPP models. The panels compare the distribution of the polarisation (a, c, d) and the autocorrelation functions of the polarisation (b, d, f) obtained from time series for the three SPP models and for their corresponding SDE.

We pause here to raise a minor point: In this study, the parameter regimes considered for the individual-based models are such that the average polarisation is high (see Section 3A). Consequently, the corresponding parameters of Eqs. 8-10 are such that $b_1 > 0$ and $c_1 > 0$, rendering the disordered state unstable. At low densities or high rate of spontaneous turning, the individual based model and the corresponding mesoscopic descriptions can give rise to disordered dynamics; the disordered state, however, is not the focus of this study.

B. Diagnostics of the discovered models

We now test if the equations that we discovered via the data-driven method capture features of the data from the spatially explicit model. We simulate the discovered equations Eqs. 8-10 using the Euler-Maruyama numerical integration scheme for Ito SDEs. In Fig. 3 top row, we find that the histogram of the order parameter for the three spatial models and the histogram for the corresponding SDE model match reasonably well. Next, as shown in Fig. 3 bottom row, the autocorrelation function of the order parameter also shows strong consistency between the original, individual-based simulations and the SDE simulations.

Finally, we also check the model consistency, as proposed by [50]. From the simulated time series generated from the original SDE estimates, we perform the data-driven estimation procedure again to re-estimate the SDE. Indeed, the re-estimated SDEs match the original estimates for each of the models. Therefore, we conclude that the data-driven discovery method has yielded reasonable mesoscopic SDEs for all the three spatial interaction models.

C. Deviations of the discovered models from their non-spatial counterparts

In the previous sections, we have observed that the discovered SDEs for both the pairwise and stochastic models are qualitatively similar to their non-spatial counterparts (compare Eq 3 to Eq 8 and Eq 4 to Eq 9-10). However, we observe a deviation from the non-spatial results in how the parameters in the SDEs change as the number of individuals in the group increases. Specifically, recall that the mesoscopic theory of the non-spatial systems predicts that the drift term does not depend on the N, while the diffusion term is inversely proportional to N (see Eq. 3-4). In our spatially explicit model with local interactions, we test this prediction about the scaling relationships of the mean-field mesoscopic theory.

We study the effect of group size on the discovered SDEs when N is varied in two different ways. The first way, which is reminiscent of how real-world experiments are done, is to vary N while keeping the arena size L constant. This approach means that the density of particles will increase with N, which makes it hard to disentangle the effect of N from density effects. As an alternative, we can vary N and L by keeping the density $\rho = N/L^2$ constant. This approach helps us to separate the effect of N from the effect of density variations. We report results from both of these approaches.

Effect of the group size on the drift term. In the non-spatial model, the drift term is independent of the group size. However, for the spatial models, we find that the coefficients of the drift term vary as a function of the group size and the density (see Fig. 4). For any fixed value of N, the drift coefficients approach the mean-field values as the interaction radius R increases. In fact, for $R \geq L/\sqrt{2}$, the model converges to the non-spatial model, and the coefficients converge to the mean-field limit.

We speculate that this dependence on N is due to the fact that the effective interaction rates in the spatial models vary as a function of N and R: this is consistent with the observation that the drift term for the pairwise interaction model—which in theory depends only on the stochastic turning rate r_0—stays independent of N for the spatial models. Below, we propose a scaling argument in order to interpret the variation of the effective parameters of the SDE models as a function of N, the density ρ, and the interacting radius R.

Effect of the group size on the diffusion term. In Fig. 5, we explore the diffusion term, and in particular its maximum value reached at $\mathbf{m} = \mathbf{0}$, $G_{xx}(0,0) = G_{yy}(0,0)$ (the maxima of the parabolas in the panels (a) to (f) of Fig. 5; see also Eqs. 8-10). Again, we either increase N while keeping the simulation arena size $L = 5$ fixed, or increase N while keeping the density $\rho = N/L^2 = 1.2$ fixed. As expected from the non-spatial models, the strength of the diffusion decreases with increasing N. However, the decay of the diffusion seems to deviate from the simple $1/N$ scaling predicted by the non-spatial models, even suggesting a possible asymptotic power-law decay $G_{xx} \sim N^{-z}$, with an exponent z which could depend on ρ and/or R. Moreover, as R increases, the $1/N$ decay is ultimately recovered.

Although anomalous exponents cannot be readily excluded, it is possible to understand the complex behaviour observed in Fig. 5 by exploiting a scaling argument describing the

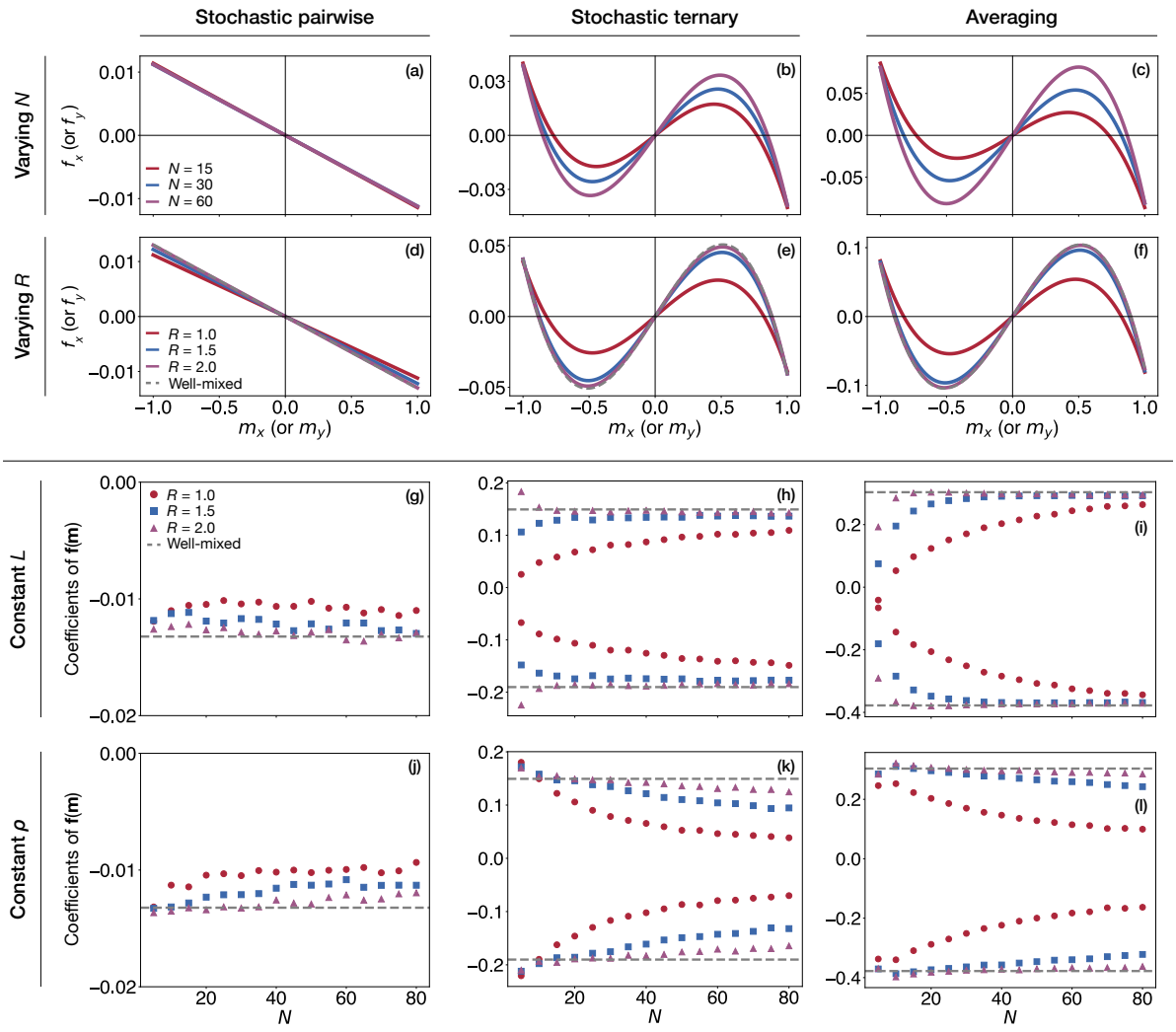

Figure 4. Dependence of the deterministic drift $\mathbf{f}(\mathbf{m})$ on N and R. In panels (a) to (f), the drift term, $f_x(\mathbf{m})$, is plotted as a function of m_x for the three models (same dependence for $f_y(\mathbf{m})$ as a function of m_y, by isotropy). (a-c) Dependence of the drift function on N for the three different models, when R is constant ($R = 1$). Deviating form the mean-field theory, the drift functions change with varying N. (d-f) Dependence of the drift function on the radius of interaction, R. As R increases, the drift functions converge to the mean-field limit ($R = \infty$). Panels (g) to (l) show the coefficients of the drift function for the 3 models (see Eqs. 8-10): $-a_1$ for the pairwise model in (g, j), $b_1 > 0$ and $-b_2 < 0$ in (h, k) for the ternary model, $c_1 > 0$ and $-c_2 < 0$ in (i, l) for the local-averaging model.In (g, h, i), N is increased while keeping the box size $L = 5$ constant, and in (j, k, l), N and L are increased simultaneously such that the density $\rho = N/L^2 = 1.2$ remains constant. For each condition in panels (g) to (l), the drift parameters are plotted for 3 different interaction radii, $R = 1.0$, 1.5 and 2.0.

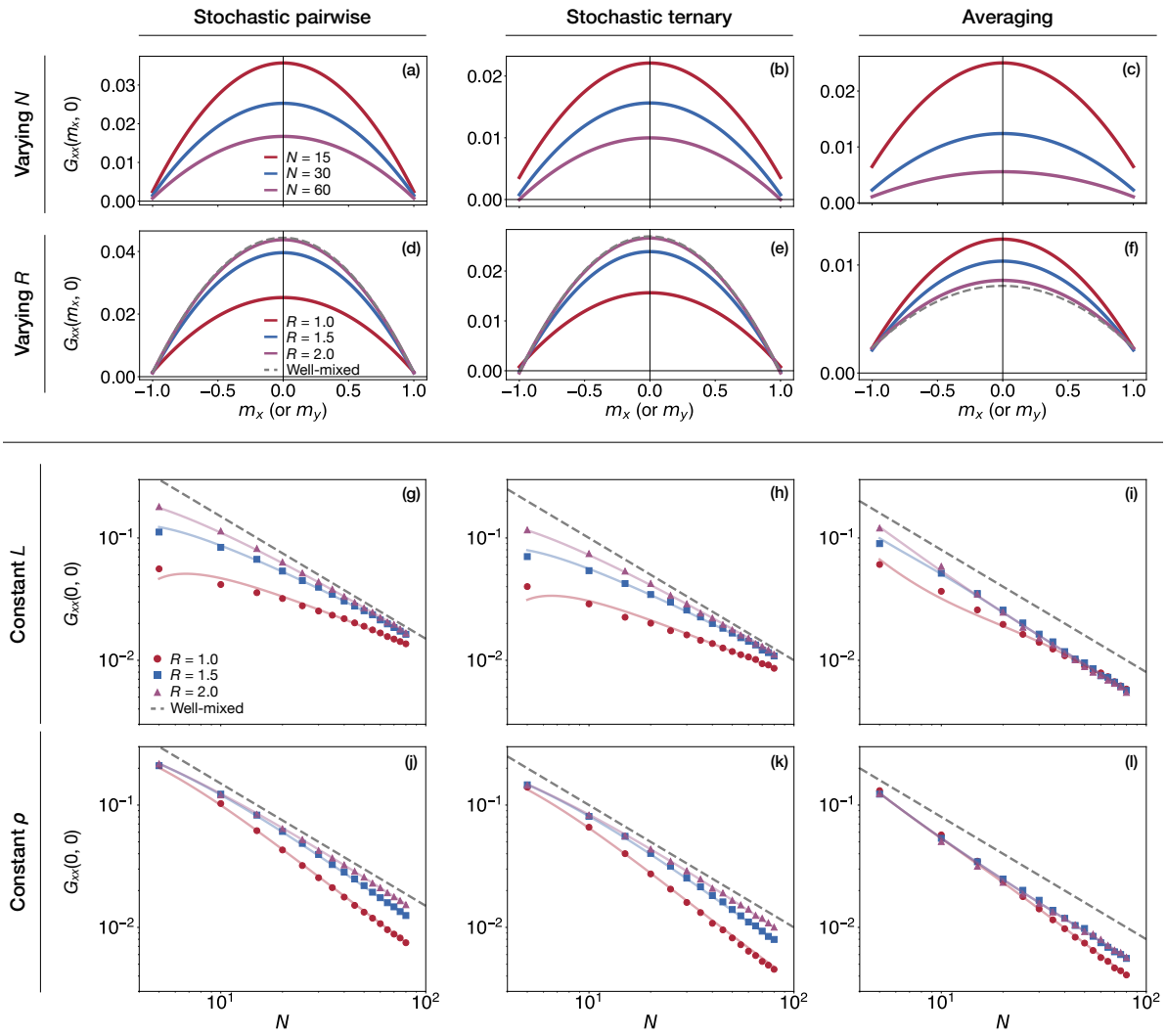

Figure 5. Dependence of the diffusion term $\mathbf{G}(\mathbf{m})$ on $N$and R. In panels (a) to (f), the diffusion, $G_{xx}(\mathbf{m}) = G_{yy}(\mathbf{m})$, is plotted as a function of $|\mathbf{m}|$ for the three models, presenting the inverse parabolic form of Eqs. 8-10. Panels (a, b, c) and (d, e, f) illustrate the dependence of the diffusion on N (for $R = 1$) and on R (for $N = 30$), respectively. In panels (g) to (l), the maximum diffusion strength, $G_{xx}(0,0) = G_{yy}(0,0)$, is plotted as a function of N for the three models. In (g, h, i), N is increased while keeping the box size $L = 5$ constant. In (j, k, l), N and L are increased simultaneously such that the density $\rho = N/L^2 = 1.2$ remains constant. For each condition, $G_{xx}(0,0)$ is plotted for 3 different interaction radii, $R = 1.0$, 1.5 and 2.0. The full lines correspond to the fit to the scaling ansatz of Eq. 11, which explains the above results in terms of a cross-over between a mean-field and a non-mean-field regime. Overall, the values of the mean number of agents in the interaction circle of radius R, $N_{\mathrm{Int}} = \pi\rho R^2$, span the interval 0.6–40. The dotted grey lines corresponds to the prediction of the mean-field (non-spatial) models.

cross-over between a mean-field regime when the interaction radius $R \gg R_c(N)$ and a regime when the mean-field results do not strictly apply, for $R \ll R_c(N)$. Here, $R_c(N)$ is a cross-over length separating these two regimes, and for a given density ρ, $R_c(N)$ is expected to increase with N. Yet, in both regimes, we will now show that our data are compatible with a diffusion term scaling like $1/N$. In fact, unless extremely long-ranged correlations are present (e.g., decaying as a small enough power-law of the distance between two agents), the law of large numbers ensures that the diffusion terms should decay like $1/N$.

Let us consider the rescaled diffusion, $g = N \times G_{xx}(0,0)$, which should be a function of N (as evident from Fig. 5) and of the dimensionless combination $N_{\text{Int}} = \pi\rho R^2$. N_{Int} can be simply interpreted as the expected number of agents in the interaction circle of radius R. We propose the scaling form

$$g(\rho R^2, N) = g_{\text{MF}} - (g_{\text{MF}} - r_0) A(\rho R^2) B(R^2/R_c^2(N)), \tag{11}$$

where A and B are 2 functions that we will strongly constrain hereafter. g_{MF} is the value taken by g for the mean-field case corresponding to the limit $N_{\text{Int}} \to \infty$ (i.e., $R \to \infty$ or $\rho \to \infty$). For instance, in the mean-field model with pairwise interactions, we have $g_{\text{MF}} = r_0 + r_1$ (see Eq. 3), whereas in the mean-field model with ternary interactions, we have $g_{\text{MF}} = r_0 + r_2$ (see Eq. 4). First, for $N_{\text{Int}} \to 0$ (i.e., $R = 0$ or $\rho \to 0$), the agents are not interacting, so that $g(0,N) = r_0$. Plugging this result in Eq. 11 imposes $A(0) \times B(0) = 1$, and we can take $A(0) = B(0) = 1$ in all generality. Moreover, from the above definition of the crossover length R_c, one should recover the mean-field result when $R \gg R_c$, and Eq. 11 imposes $\lim_{u\to\infty} B(u) = 0$. Finally, at fixed ρ and R and in the limit $N \to \infty$, we have $B(R^2/R_c^2(N)) \to B(0) = 1$, and the rescaled diffusion becomes independent of N and takes the asymptotic form

$$g(\rho R^2, \infty) = g_{\text{MF}} - (g_{\text{MF}} - r_0) A(\rho R^2). \tag{12}$$

Hence, the function A encodes the dependence of the rescaled diffusion on ρR^2, in the $N \to \infty$ limit. Of course, if we now take the limit $\rho R^2 \to \infty$, $g(\rho R^2, \infty)$ must go to g_{MF}, and Eq. 11 imposes $\lim_{u\to\infty} A(u) = 0$.

In order to fit the results of Fig. 5 by exploiting Eq. 11 and using as few fitting parameters as possible, we assume simple forms of the functions A and B, compatible with the constraints that we obtained above. For the pairwise model and ternary models, we have used $A(u) = \exp(-au)$ and $B(u) = \exp(-bu)$, where a and b are model-dependent fitting constants. In addition, we have assumed a natural power law growth, $R_c(N) \sim N^{\alpha/2}/\sqrt{\rho}$, for the cross-over length. Interestingly, our fitting procedure resulted in the same $\alpha \approx 0.8$ for both models. The reduced variable $R^2/R_c^2(N)$ appearing in Eq. 11 can be rewritten as

$$\frac{R^2}{R_c^2(N)} = \frac{\pi\rho R^2}{\pi\rho R_c^2(N)} \sim \frac{N_{\text{Int}}}{N^\alpha}. \tag{13}$$

The model is effectively in the mean-field regime only when $R \gg R_c(N)$, i.e., $N_{\text{Int}} \gg N^\alpha$, and the diffusion term then behaves like $G_{xx}(0,0) = g_{\text{MF}}/N$. Otherwise, for $R \ll R_c(N)$ (or equivalently, $N_{\text{Int}} \ll N^\alpha$), we have $G_{xx}(0,0) = g(\rho R^2, \infty)/N$, where $g(\rho R^2, \infty)$ is given by Eq. 12. Finally, for the model where the focal agent interacts with all other agents in the

interacting circle, we find $\alpha \approx 0.4$, about half the value of the exponent for the binary and ternary interaction models.

The result of our fitting procedure is presented in Fig. 5 and shows a fair agreement between the model simulations and the scaling ansatz of Eq. 11, and without too much effort in optimising the functional form of A and B to improve the fit (to keep as few fitting parameters as possible), which would anyway require to explore much larger values of N and a wider range of N_{Int}. Again, the main purpose of this section was to make plausible the fact the diffusion scales like $1/N$, and that the complex behaviour of the diffusion observed in Fig. 5 can be interpreted by a scaling argument as a cross-over between a mean-field regime and a non mean-field regime.

5. Discussion

In this manuscript, we obtained mesoscopic (i.e. small-group sized) descriptions of a simple spatially-explicit local-alignment-based model of collective motion. To do so, we adopted a novel data-driven equation discovery approach [66, 65]. For the class of spatial models we considered, a focal individual interacts with k randomly chosen neighbours within a radius R. Our results reveal broad consistency between the mean-field theory and the spatially explicit models. However, a novel finding of our analysis is that the scaling relationship between the diffusion term or strength of noise $\mathbf{G}$, and the group size N for spatial models can depart substantially from the mean-field theory. In particular, the considered range of N and $N_{\text{Int}} = \pi\rho R^2$ (the mean number of agents in the interaction circle of radius R) appears to have a strong impact on the scaling of the diffusion $\mathbf{G}$.

Our study offers insights on the collective motion of small to intermediate-sized animal groups, which have not been emphasised well enough in the literature. Much of the physics literature has focused on the thermodynamic or macroscopic limit [3, 1, 19, 20]. In contrast, we focus on understanding mesoscale descriptions of biologically inspired variants of a classic collective motion model, with group polarisation as the order parameter of interest. The data-driven mesoscopic description of the order parameter yields stochastic differential equations, containing deterministic (called drift) and stochastic (called diffusion) terms. The analysis of these terms reveals that the nature of collective order at the mesoscale arising from stochastic pairwise interactions ($k = 1$ in our model) and stochastic ternary/higher-order interactions (i.e., $k \geq 2$ in the model) are fundamentally different. More specifically, we find that the stochastic pairwise interactions can lead to ordered collective motion at mesoscopic scales; this is due to intrinsic noise, i.e., noise arising from finite-sized systems. Earlier theoretical studies have also emphasised the role of noise in creating new states [34]. Reynolds et. al. [41, 42] later confirmed these predictions empirically. While these studies included multiplicative noise at the individual level, it only arises at the group level in our case. In contrast, for stochastic ternary or the higher order interaction models, including the Vicsek averaging interactions, the collective order is driven by the deterministic terms in the mesoscopic description; hence, the role of noise is secondary. These results of the spatially-explicit model with local interactions are broadly consistent with the previous mean-field

theories and simulations of the collective behaviour models that ignore spatial effects.

Our analysis also reveals departures between the mean-field theory and spatial models when we consider the scaling relationships of the mesoscopic equations, i.e. how the drift and diffusion terms depend on the population size N. Mean field theory predicts that the drift term must be independent of N. For our spatial model, although the qualitative nature (i.e., functional form) of the drift is independent of N, we find that the quantitative features of the data-derived drift term do depend on N. Mean-field theory also predicts that diffusion $\mathbf{G}$ is inversely proportional to the population size N. In contrast, we find that this relationship follows an apparent power-law $G \sim N^{-z}$ for a range of N and N_{Int}, where z can be substantially smaller than 1 when the radius of local interaction is small. We introduced a simple scaling argument which interprets this phenomenon as a cross-over between a non mean-field regime (when $N_{\text{Int}} \ll N^{\alpha}$) and a mean-field regime (when $N_{\text{Int}} \gg N^{\alpha}$). Ultimately, for a given density and radius R, and hence $N_{\text{Int}} = \pi\rho R^2$, our analysis indeed suggests that $G \sim g(N_{\text{Int}})/N$ scales like $1/N$ like in the mean-field models, albeit with a constant $g(N_{\text{Int}})$ depending on N_{Int}.

The above results could be discussed in light of empirical results of karimeen (*Etroplus suratensis*) [28] where authors found that $z = 1$ well approximates the data, for a range of group sizes (15 to 60). Real fish are naturally extended in space, and they do not interact with all neighbours. Hence, it is interesting that these empirical data match the simpler mean-field theoretical expectation rather than the prediction of our spatially explicit model! We speculate two possible reasons for the empirical finding: First, it is possible that the radius of interactions among fish is already large enough for to converge to the mean-field expectations. A second possibility is that the Vicsek class of models are too simplistic for real-world applications. We add that these two possibilities are not necessarily mutually exclusive. We stress that further studies – via simulations, theory, and real-data analysis – are needed to understand how space and the complexity of interactions among agents affect the deviations from the mean-field mesoscopic theory.

We now ask if the stochastic pairwise copying of neighbours – i.e., interacting with only one neighbour at a time – over a period of time can be approximated as locally averaging. Both our mean field mesoscopic theory and data-driven mesoscopic equations clearly show that stochastic pairwise ($k = 1$ in our model) and higher-order interactions ($k \geq 2$) are fundamentally different. The drift term for the stochastic pairwise is linear with disorder as the stable equilibrium; any observed collective order, therefore, is noise-induced. In the macroscopic limit ($N \to \infty$), this system admits only disorder. On the other hand, the drift term for the higher-order interactions is cubic, resulting in an unstable disordered state ($\mathbf{m} = 0$) and a stable ordered state ($|\mathbf{m}| \approx 1$) when the rate of ternary interactions are higher than the rate of spontaneous turning. In the macroscopic limit ($N \to \infty$), this system admits order, which is typical of the Vicsek-class of collective motion models. Thus, the collective order in this model is primarily driven by deterministic forces. Hence, the governing equations and the dynamics of collective motion driven by stochastic pairwise and higher-order interactions are not equivalent either at the microscopic or at the group level.

Finally, we make remarks about inferring local interactions among organisms based on the data-driven characterisation of the group-level dynamics captured as a stochastic

differential equation, as suggested by [50]. This is an attractive proposition, since it is really difficult, if not impossible, to infer the local interactions that an organism follows from group-level data [75], like time series for the group polarisation [28, 58]. Based on the fact that drift functions are qualitatively different between stochastic pairwise and higher-order interactions, we may be able to distinguish between these two possibilities even if we only have group-level mesoscopic equations. However, our analysis suggests that ternary and local-averaging (involving multiple, time varying number of interactions) both yield qualitatively similar drift function. Hence, there are fundamental limits to what we can infer about local interactions based on mesoscopic equations alone.

6. Concluding remarks

Deriving mean-field descriptions of collective systems is a non-trivial undertaking, even for highly simplified theoretical models. At mesoscopic scales, where one needs to incorporate finite-size effects and stochasticity, deriving mean-field models by hand becomes prohibitive even for relatively simple models. Therefore, we propose a data-driven approach to *discover* the mesoscopic SDE models directly from simulated data. As we showed in this manuscript, even for a relatively simple class of collective motion models that accounted only for alignment interactions, we discovered some deviations from the mean-field theory. Real animal groups likely exhibit additional interactions, such as attraction and repulsion, and may have more complex interaction mechanisms. There are several models in the literature that aim to capture more realistic animal behaviour [16, 29, 76, 77, 78]. For such models, we argue that there is a massive potential to discover the mesoscopic equations for a variety of both toy models of collective motion as well as models of collective motion that account for detailed behaviours of the organisms. Indeed, for real-world systems, the data-derived stochastic dynamical equation is a powerful approach that may uncover the role of deterministic and stochastic forces in shaping the collective dynamics. Our approach is general enough to be applied to both real datasets and complicated models of collective motion, although care should be taken in choosing appropriate order parameter and the functional forms for the mesoscopic equations, and eventually, in interpreting the results. While we focused on stochastic dynamics of group polarisation with no external perturbations, it would be interesting to apply the equation-discovery approaches to study responses of groups to perturbations [10, 38], for example, mimicking predatory attack or other biologically relevant scenarios. We hope our study inspires development of further theory, simulations as well as real data applications of these broad ideas.

Code availability

The code for the agent-based model simulations (MATLAB) and the data-driven SDE discovery pipeline (Python) are available on the GitHub repository: `https://github.com/tee-lab/data-driven-mesoscale-sde`. (DOI: `https://doi.org/10.5281/zenodo.8088825`)

Acknowledgements

VG and GT acknowledge the support of the Indo-French Centre for the Promotion of Advanced Research (project N°64T4-B), VG from the Science and Engineering Research Board, AN from the Ministry of Education for PhD scholarship, VJ from Prime Minister's Research Fellowship program, and DRM from Department of Science and Technology (DST) INSPIRE-Faculty award. GT also gratefully acknowledges the Indian Institute of Science for support via Infosys Visiting Chair Professor at the Centre for Ecological Sciences, IISc, Bengaluru.

References

[1] Ramaswamy S 2010 *Annu. Rev. Condens. Matter Phys.* **1** 323–345
[2] Ramaswamy S 2017 *Journal of Statistical Mechanics: Theory and Experiment* **2017** 054002
[3] Vicsek T and Zafeiris A 2012 *Physics Reports* **517** 71–140
[4] Sumpter D J 2010 *Collective Animal Behavior* (Princeton University Press)
[5] Camazine S, Deneubourg J L, Franks N R, Sneyd J, Theraulaz G and Bonabeau E 2001 *Self-Organization in Biological Systems* (Princeton University Press)
[6] Vásárhelyi G, Virágh C, Somorjai G, Nepusz T, Eiben A E and Vicsek T 2018 *Science Robotics* **3** eaat3536
[7] Bürkle A, Segor F and Kollmann M 2011 *Journal of Intelligent & Robotic Systems* **61** 339–353
[8] Berlinger F, Gauci M and Nagpal R 2021 *Science Robotics* **6** eabd8668
[9] Ouellette N T 2022 *Physical Biology* **19** 021004
[10] Ouellette N T 2019 *Matter* **1** 297–299
[11] Deutsch A, Friedl P, Preziosi L and Theraulaz G 2020 *Philosophical Transactions of the Royal Society B* **375** 20190377
[12] Deutsch A, Theraulaz G and Vicsek T 2012 *Interface Focus* **2** 689–692
[13] Huth A and Wissel C 1992 *Journal of Theoretical Biology* **156** 365–385
[14] Aoki I 1982 *Bull. Jpn. Soc. Sci. Fish* **48** 1081–1088
[15] Vicsek T, Czirók A, Ben-Jacob E, Cohen I and Shochet O 1995 *Physical Review Letters* **75** 1226–1229 ISSN 0031-9007, 1079-7114 URL `https://link.aps.org/doi/10.1103/PhysRevLett.75.1226`
[16] Couzin I D, Krause J, James R, Ruxton G D and Franks N R 2002 *Journal of Theoretical Biology* **218** 1–11
[17] Hemelrijk C K and Kunz H 2005 *Behavioral Ecology* **16** 178–187
[18] Calovi D S, Lopez U, Ngo S, Sire C, Chaté H and Theraulaz G 2014 *New Journal of Physics* **16** 015026
[19] Toner J and Tu Y 1995 *Physical Review Letters* **75** 4326
[20] Toner J and Tu Y 1998 *Physical Review E* **58** 4828
[21] Czirók A, Barabási A L and Vicsek T 1999 *Physical Review Letters* **82** 209
[22] Romanczuk P and Schimansky-Geier L 2012 *Ecological Complexity* **10** 83–92
[23] Grossmann R, Schimansky-Geier L and Romanczuk P 2012 *New Journal of Physics* **14** 073033
[24] Boettiger C 2018 *Ecology Letters* **21** 1255–1267
[25] Bertin E, Chaté H, Ginelli F, Mishra S, Peshkov A and Ramaswamy S 2013 *New Journal of Physics* **15** 085032
[26] Majumder S, Das A, Kushal A, Sankaran S and Guttal V 2021 *The European Physical Journal Special Topics* **230** 3389–3401
[27] Tunstrøm K, Katz Y, Ioannou C C, Huepe C, Lutz M J and Couzin I D 2013 *PLoS Computational Biology* **9** e1002915
[28] Jhawar J, Morris R G, Amith-Kumar U, Danny Raj M, Rogers T, Rajendran H and Guttal V 2020 *Nature Physics* **16** 488–493
[29] Calovi D S, Litchinko A, Lecheval V, Lopez U, Pérez Escudero A, Chaté H, Sire C and Theraulaz G 2018 *PLoS Computational Biology* **14** e1005933

[30] Lei L, Escobedo R, Sire C and Theraulaz G 2020 *PLoS Computational Biology* **16** e1007194
[31] Gautrais J, Ginelli F, Fournier R, Blanco S, Soria M, Chaté H and Theraulaz G 2012 *PLOS Computational Biology* **8** 1–11 URL https://doi.org/10.1371/journal.pcbi.1002678
[32] Herbert-Read J E, Perna A, Mann R P, Schaerf T M, Sumpter D J and Ward A J 2011 *Proceedings of the National Academy of Sciences* **108** 18726–18731
[33] Katz Y, Tunstrøm K, Ioannou C C, Huepe C and Couzin I D 2011 *Proceedings of the National Academy of Sciences* **108** 18720–18725
[34] Okubo A 1986 *Advances in biophysics* **22** 1–94
[35] Reynolds A M and Ouellette N T 2016 *Scientific reports* **6** 30515
[36] Reynolds A M 2021 *The European Physical Journal E* **44** 1–6
[37] Jhawar J, Morris R G and Guttal V 2019 Deriving Mesoscopic Models of Collective Behavior for Finite Populations *Handbook of Statistics* vol 40 (Elsevier) pp 551–594 ISBN 978-0-444-64152-6
[38] Ni R, Puckett J G, Dufresne E R and Ouellette N T 2015 *Physical review letters* **115** 118104
[39] Ni R and Ouellette N T 2016 *Physical biology* **13** 045002
[40] Reynolds A 2018 *Journal of The Royal Society Interface* **15** 20170806
[41] Reynolds A M 2019 *Physical biology* **16** 046002
[42] Reynolds A M 2021 *Scientific Reports* **11** 1–12
[43] Reynolds A M 2023 *Physical Biology* **20** 025002
[44] Jadhav V, Guttal V and Masila D R 2022 *Royal Society Open Science* **9** 220124
[45] Joshi J, Couzin I D, Levin S A and Guttal V 2017 *PLoS Computational Biology* **13** e1005732
[46] Joshi J and Guttal V 2018 *Evolution* **72** 2595–2607
[47] Biancalani T, Dyson L and McKane A J 2014 *Physical Review Letters* **112** 038101
[48] Yates C A, Erban R, Escudero C, Couzin I D, Buhl J, Kevrekidis I G, Maini P K and Sumpter D J T 2009 *Proceedings of the National Academy of Sciences* **106** 5464–5469 ISSN 0027-8424, 1091-6490 URL https://pnas.org/doi/full/10.1073/pnas.0811195106
[49] Dyson L, Yates C A, Buhl J and McKane A J 2015 *Phys. Rev. E* **92**(5) 052708 URL https://link.aps.org/doi/10.1103/PhysRevE.92.052708
[50] Jhawar J and Guttal V 2020 *Philosophical Transactions of the Royal Society B* **375** 20190381
[51] Chatterjee P and Goldenfeld N 2019 *Physical Review E* **100** 040602
[52] Gardiner C 1985 *Handbook of Stochastic Methods* vol 4 (Springer Berlin, 2009)
[53] Horsthemke W and Lefever R 1989 *Noise in Nonlinear Dynamical Systems* **2** 179
[54] Narayan V, Ramaswamy S and Menon N 2007 *Science* **317** 105–108
[55] Nair G G, Senthilnathan A, Iyer S K and Guttal V 2019 *Physical Review E* **99** 032412
[56] Jiang L, Giuggioli L, Perna A, Escobedo R, Lecheval V, Sire C, Han Z and Theraulaz G 2017 *PLoS Computational Biology* **13** e1005822
[57] Hinz R C and de Polavieja G G 2017 *Proceedings of the National Academy of Sciences* **114** 2295–2300
[58] Puckett J G, Ni R and Ouellette N T 2015 *Physical Review Letters* **114** 258103
[59] Beleyur T and Goerlitz H R 2019 *Proceedings of the National Academy of Sciences* **116** 26662–26668
[60] Lemasson B H, Anderson J J and Goodwin R A 2009 *Journal of Theoretical Biology* **261** 501–510
[61] Lemasson B H, Anderson J J and Goodwin R A 2013 *Proceedings of the Royal Society B: Biological Sciences* **280** 20122003
[62] Calvao A M and Brigatti E 2014 *PLoS One* **9** e94221
[63] Camperi M, Cavagna A, Giardina I, Parisi G and Silvestri E 2012 *Interface focus* **2** 715–725
[64] Li Y J, Wang S, Han Z L, Tian B M, Xi Z D and Wang B H 2011 *Europhysics Letters* **93** 68003
[65] Nabeel A, Karichannavar A, Palathingal S, Jhawar J, Danny Raj M and Guttal V 2022 *arXiv preprint arXiv:2205.02645*
[66] Brunton S L, Proctor J L and Kutz J N 2016 *Proceedings of the National Academy of Sciences* **113** 3932–3937
[67] Callaham J L, Loiseau J C, Rigas G and Brunton S L 2021 *Proceedings of the Royal Society A* **477** 20210092
[68] Durrett R and Levin S 1994 *Theoretical Population Biology* **46** 363–394

[69] Bode N W, Franks D W and Wood A J 2010 *Journal of Theoretical Biology* **267** 292–299
[70] Strömbom D, Hassan T, Hunter Greis W and Antia A 2019 *Royal Society Open Science* **6** 190381
[71] Gillespie D T 1976 *Journal of Computational Physics* **22** 403–434
[72] Gillespie D T 1977 *The Journal of Physical Chemistry* **81** 2340–2361
[73] Tabar R 2019 *Analysis and Data-Based Reconstruction of Complex Nonlinear Dynamical Systems* vol 730 (Springer)
[74] Gorjão L R and Meirinhos F 2019 *Journal of Open Source Software* **4** 1693
[75] Nabeel A and Masila D R 2022 *Chaos: An Interdisciplinary Journal of Nonlinear Science* **32** 063119
[76] Wang W, Escobedo R, Sanchez S, Sire C, Han Z and Theraulaz G 2022 *PLoS Computational Biology* **18** e1009437
[77] Haluts A, Reyes S F G, Gorbonos D, Etheredge R I, Jordan A and Gov N S 2021 *Proceedings of the National Academy of Sciences* **118** e2106269118
[78] Haluts A, Jordan A and Gov N S 2022 *arXiv preprint arXiv:2211.16542*